AFRL-IF-RS-TR-2005-371
Final Technical Report
November 2005

RADIO FREQUENCY (RF) BIOMOLECULES

MIT Media Laboratory

Sponsored by
Defense Advanced Research Projects Agency
DARPA Order No. M298

AIR FORCE RESEARCH LABORATORY
INFORMATION DIRECTORATE
ROME RESEARCH SITE
ROME, NEW YORK

STINFO FINAL REPORT

This report has been reviewed by the Air Force Research Laboratory, Information Directorate, Public Affairs Office (IFOIPA) and is releasable to the National Technical Information Service (NTIS). At NTIS it will be releasable to the general public, including foreign nations.

AFRL-IF-RS-TR-2005-371 has been reviewed and is approved for publication

APPROVED: /s/
THOMAS RENZ
Project Engineer

FOR THE DIRECTOR: /s/
JAMES A. COLLINS, Deputy Chief
Advanced Computing Division
Information Directorate

REPORT DOCUMENTATION PAGE

Form Approved
OMB No. 074-0188

1. AGENCY USE ONLY (Leave blank)	2. REPORT DATE	3. REPORT TYPE AND DATES COVERED
	November 2005	**Final** **Sep 01 – Oct 04**

4. TITLE AND SUBTITLE

RADIO FREQUENCY (RF) BIOMOLECULES

5. FUNDING NUMBERS

G - F30602-01-2-0596
PE - 61101E
PR - BIOC
TA - M2
WU - 98

6. AUTHOR(S)

Joseph Jacobson

7. PERFORMING ORGANIZATION NAME(S) AND ADDRESS(ES)

MIT Media Laboratory
20 Ames Street
Cambridge MA 02139

8. PERFORMING ORGANIZATION REPORT NUMBER

N/A

9. SPONSORING / MONITORING AGENCY NAME(S) AND ADDRESS(ES)

Defense Advanced Research Projects Agency
3701 North Fairfax Drive
Arlington VA 22203-1714

AFRL/IFTC
525 Brooks Road
Rome NY 13441-4505

10. SPONSORING / MONITORING AGENCY REPORT NUMBER

AFRL-IF-RS-TR-2005-371

11. SUPPLEMENTARY NOTES

AFRL Project Engineer: Thomas Renz/IFTC/(315) 330-3423 Thomas.Renz@rl.af.mil

12a. DISTRIBUTION / AVAILABILITY STATEMENT

APPROVED FOR PUBLIC RELEASE; DISTRIBUTION UNLIMITED.

12b. DISTRIBUTION CODE

13. ABSTRACT ***(Maximum 200 Words)***

This report details the results of the MIT RF Biology Program. The RF Biology Program represents an effort to imbue electronic functionality to biomolecules and a means for synthesizing electronically active biomolecules.

14. SUBJECT TERMS

DNA Computing, Biocomputing, RF Molecules

15. NUMBER OF PAGES 21

16. PRICE CODE

17. SECURITY CLASSIFICATION OF REPORT	18. SECURITY CLASSIFICATION OF THIS PAGE	19. SECURITY CLASSIFICATION OF ABSTRACT	20. LIMITATION OF ABSTRACT
UNCLASSIFIED	UNCLASSIFIED	UNCLASSIFIED	UL

Table of Contents

List of Figures

Preface

The Radio Frequency (RF) Biology program was developed by the Massachusetts Institute of Technology Media Laboratory (MIT Media Lab) under the program management of the DARPA–IPTO Office (Dr. Sri Kumar) and the Air Force Research Laboratory Information Technology Directorate (Dave Williamson, Dr. Tom Renz). The purpose of this program was to develop electronically active bio-molecules. These nano-particles could be the key to successful molecular scale electronics.

Summary

Under this program a general approach was developed for synthesizing biomolecules with electronic properties. The approach involved the preparation of nucleic acids or amino acid building blocks monofunctionalized with metallic nanoparticles. This enabled remote electronic control of the hybridization behavior of synthetic DNA. The control was achieved by inductive coupling to a Radio Frequency Magnetic Field, RFMF, through the metallic nanoparticles. The absorbed energy was transduced into heat which caused melting, or denaturation, of the DNA molecule. The highly localized nature of the heating effect left surrounding molecules relatively unaffected.

The program began with the creation of RFMF susceptible DNA/nanoparticle ensembles described in Section 3.1. It then focused on creation and attachment of nanoparticles that incorporated resonance into the coupling mechanism for better efficiency and individual molecule selectivity, (Section 3.2). Section 3.3 focuses on the development of NanoPearls, electronic amino acid building blocks for functional electronic circuitry.

Two papers which describe the synthesis of gold, Au, nanoparticles and their use as RFMF antennas for this project are given in the appendix.

1. Introduction and Background

Over the past several years it has become increasingly possible to design a one dimensional string of either nucleic acid or amino acid building blocks such that the string then folds into a known and useful three dimensional structure (i.e. aptamer or peptide respectively). That being said DNA, RNA or protein structures constructed from naturally occurring building blocks, either nucleic acids or amino acids respectively, do not display significant electronic properties.

The goal of the RF Biomolecules program was to layout a general approach towards creating a set of molecular scale building blocks which possess electronic properties and to indicate some potential applications.

2. Technical Approach

The technical approach is broken down into 3 areas presented in the results section below: Section 3.1 Electronically active DNA structures, Section 3.2 Orthogonal (magnetic) control channels, and Section 3.3 Building blocks for creating proteins with electronically active elements. The two papers in the Appendix describe the Section 3.1 work in more technical detail.

3. Results and Discussion

3.1 Electronically Active DNA Structures

It was reported that a DNA molecule with a 1.4nm Au nanoparticle covalently attached to it could be selectively dehybridized in a 1GHz Radio Frequency Magnetic Field, RFMF [1 and Appendix]. The RFMF coupled into the nanoparticle and locally heated the bio-molecule while the global temperature of the solution remained constant. **Figure 1** shows an ultra violet time-course spectrum (260nm) of a DNA hairpin-loop structure in which the DNA hybridization state followed that of the RFMF on/off cycle. A_{260} along the y axis is the absorbance of the hairpin loops shown at the right of the figure. The top graph corresponds to the top DNA loops, which had a Au nanoparticle attached, (squares). The bottom graph corresponds to the behavior of the same hairpin loops but without the nanoparticles, (circles). The hairpin-loop is a 38mer with a seven base-pair complement.

While the mechanism of local heat generation was not yet elucidated at the writing of this report, it was proposed that the RFMF inductively heated the metallic nanoparticle. Given this proposed mechanism, there was no resonance frequency at which the DNA dehybridized, rather, there was a threshold / basement frequency at 800MHz, above which the localized heating occurred. **Figure 2** illustrates the selective dehybridization of DNA in a RFMF.

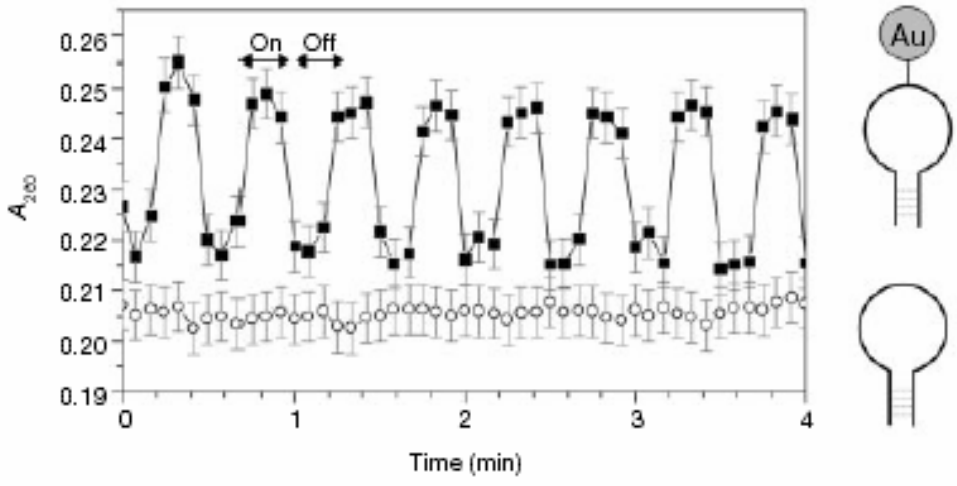

Figure 1. Selective dehybridization of a DNA hairpin-loop by coupling 1GHz RFMF into covalently attached 1.4nm Au55 antennae [1].

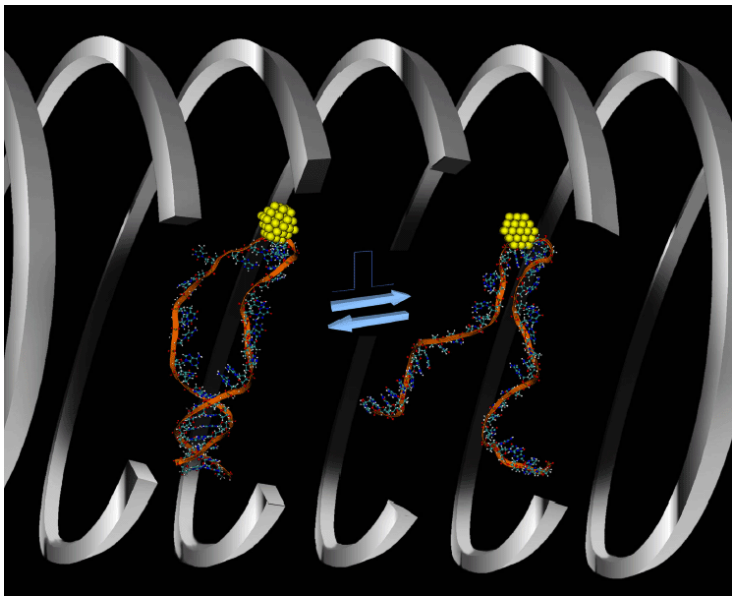

Figure 2. Illustration of selective dehybridzation of a DNA hairpin-loop by RFMF. Image courtesy of Dr. Won-Muk Hwang, MIT Center for Biomedical Engineering.

3.2 Orthogonal (Magnetic) Control Channels

The next portion of the project was directed towards synthesizing nanoparticles with resonant RFMF absorption bands so that many biological molecules could be independently addressed in solution. In the experimental work described here, covalently attached 2.8nm ε-phase cobalt nanoparticles were created as antennae because superparamagnetic nanoparticles exhibit resonant absorption bands in the RFMF that depend on chemical composition and nanoparticle size [2]. In the MHz frequency regime, these resonant losses are known as Neél losses.

Imaging Details:

High-resolution Transmission Electron Micrographs were attained using a JEOL 2010 TEM on copper/Formvar grids from Ladd Research Incorporated. Fourier Transform Infrared Spectroscopy, FTIR, data was taken using a Digi-Lab Excalibur FTS 3000 instrument (KBr, 64 scans, 4cm^{-1} resolution). Fluorescence spectra were obtained using a Jovin-Ybon Spex Fluoromax-3 spectrophotometer (3mm x 3mm quartz cuvette, 1nm slits, 0.5s integration).

Cobalt Nanoparticle Synthesis:

Cobalt nanoparticle synthesis was based on the synthesis reported by Murray and Sun [4]. The synthesis was performed under nitrogen. Cobalt chloride (CoCl2, 1.0mmol) and 11-aminoundecanoic acid (2.0mmol) were added in octyl ether (20mL, 0.05MCo) and heated to 100°C. Tri(octyl)phosphine (3.0mmol) was added, and the solution was heated to 160°C. 1.0M Super-Hydride in THF (2.0mL, 2.0mmol) was added and the solution was stirred vigorously for 20 minutes; the solution color

immediately changes from "cobalt blue" to black. Additional Super-Hydride was added (1.0mL, 1.0mmol), and the solution was stirred for 20 minutes. The mixture was then slowly cooled to room temperature and then removed from the nitrogen atmosphere. The nanoparticles were purified by centrifugation in pure ethanol two times, (approximately 3mg/mL) for 2 hours at 6000g followed by decantation and then air-dried.

Covalent attachment of cobalt nanoparticles to DNA hairpin-loop:

The DNA hairpin-loop, **Figure 3,** ("stem-loop" or "molecular beacon") was synthesized by Genset Oligos. The terminal nucleotides made up a 7-base-pair stem, with a 24-base-pair loop. The fluorescein dye, FAM, was appended at the 5' end, and the quencher, Dabcyl, at the 3' end. The eighteenth base, denoted as T', was a thymine with an internally modified free amine. The sequence of the oligonucleotide is (5' $\rightarrow$ 3') given below with the portion in parenthesis representing the "loop" of the hairpin-loop structure:

FAM – GCGCCCT – (AAACTGGTGGT'GGAATGCGTCATG) – AGGGCGC – Dab

The coupling and purification strategy is shown in **Figure 3**. Upon receiving the oligonucleotides, a 30μm stock solution was made in dimethyl sulfoxide, DMSO. To obtain carboxylic acid functionalized hairpin-loops, 100μL of the stock solution (3nmol) was shaken overnight with 100μL chloroacetic acid in DMSO (300μM) (10x, 30nmol) at room temperature, using standard nitrogen techniques. The oligonucleotide was purified by overnight ethanol precipitation and then redispersed in 500μL DMSO. A tenfold excess of cobalt nano-particles (3mg, approximately 30nmol) and a large excess of ethyldiethylaminopropylcarbodiimide (EDC) were added and the solution was shaken overnight. The sample was lyophilized, and then purified by overnight ethanol precipitation. The DNA/nanoparticle assembly was recast in 1x phosphate buffered saline, PBS buffer, to make a 1μM solution.

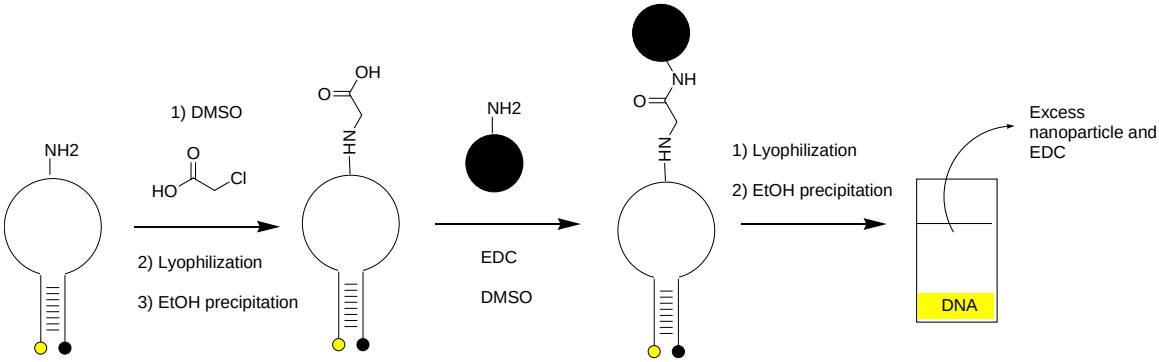

Figure 3. Coupling and purification strategy of covalent attachment of cobalt to DNA hairpin-loop.

3.3 NanoPearls: Building Blocks for Creating Peptides with Electronically Active Elements

To date the approaches for adding electronic function, such as nanoparticles to protein systems, consists of either creating proteins with a cysteine group, to which a single type of nanoparticle can be added after the fact, or employing peptides (i.e. naturally occurring phytochelatans) which can synthesize a particular type of nano-particle in situ. The first approach is greatly limited in that one can build with only a single type of nanoparticle. The second approach is equally limited in that one cannot build the type of complex three dimensional (tertiary structure) electronic assemblies needed to build functional circuitry.

The first steps towards creating electronic amino acid building blocks were demonstrated. The process consisted of multiple electronic elements including metals and semiconductors which are directly ligatable to form chains which can then fold to form an entire 'electronic protein'. The elegance of this idea is that by creating the appropriate 1 dimensional ordering of nano electronic parts, upon folding, the appropriate parts come into 3 dimensional registration with each other to make a complex electronic device. The parts were designed to be ligated not only in vitro synthesis, such as on a peptide synthesizer as originally proposed in the first phase of this project, but also in vivo, which was to be undertaken in the project's second phase. As an ultimate goal, non-biochemical building blocks were envisioned to make completely new types of protein like entities (1 dimension -> 3 dimension folding) but with vastly different properties. The addition of electronic functionality to the set of what biology itself can fabricate greatly expands the capability of de novo engineered biological constructs.

There were two main goals for the Nanopearls project.

- *Hybrid Amino Acid – Electronic Building Blocks for Directly Creating Protein Like Structures with Electronic Function*

- *Synthesized on a Peptide Synthesizer or Ultimately In-Vivo*

Figure 4 shows a library of amino acid building blocks with electronic functionality. A schematic diagram of a peptide constructed with electronic elements is also shown. **Figure 5** lays out the synthetic steps and initial results towards creating electronically active amino acid building blocks [5]. The full synthesis is detailed in Reference 5.

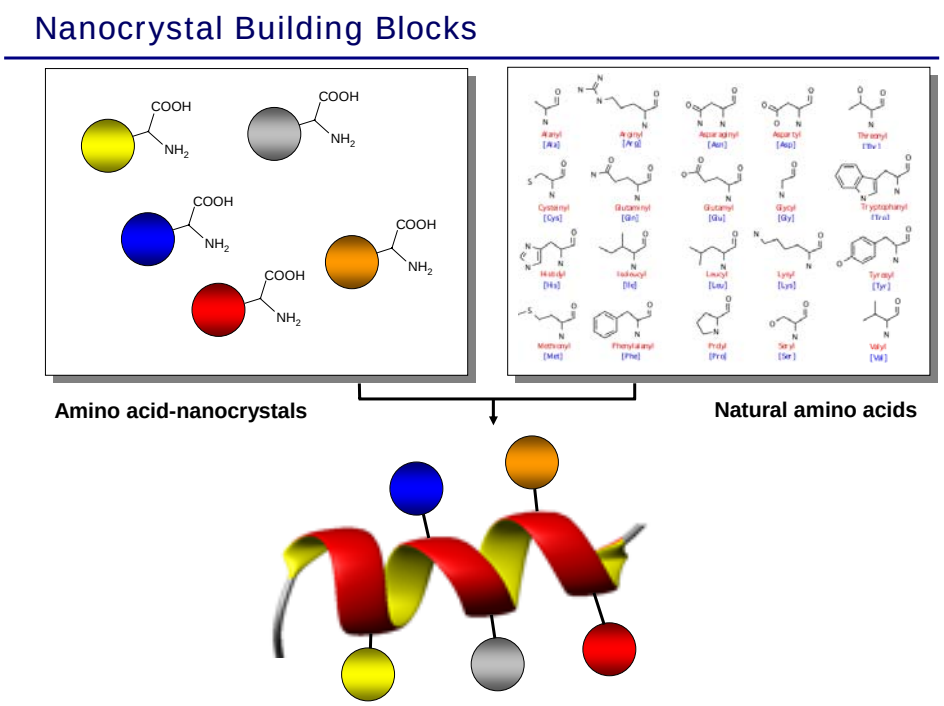

Figure 4. Schematic Diagram of Amino Acid Library with Nanocrystal Building Blocks for Creating Programmable Peptides with Electronic Functionality.

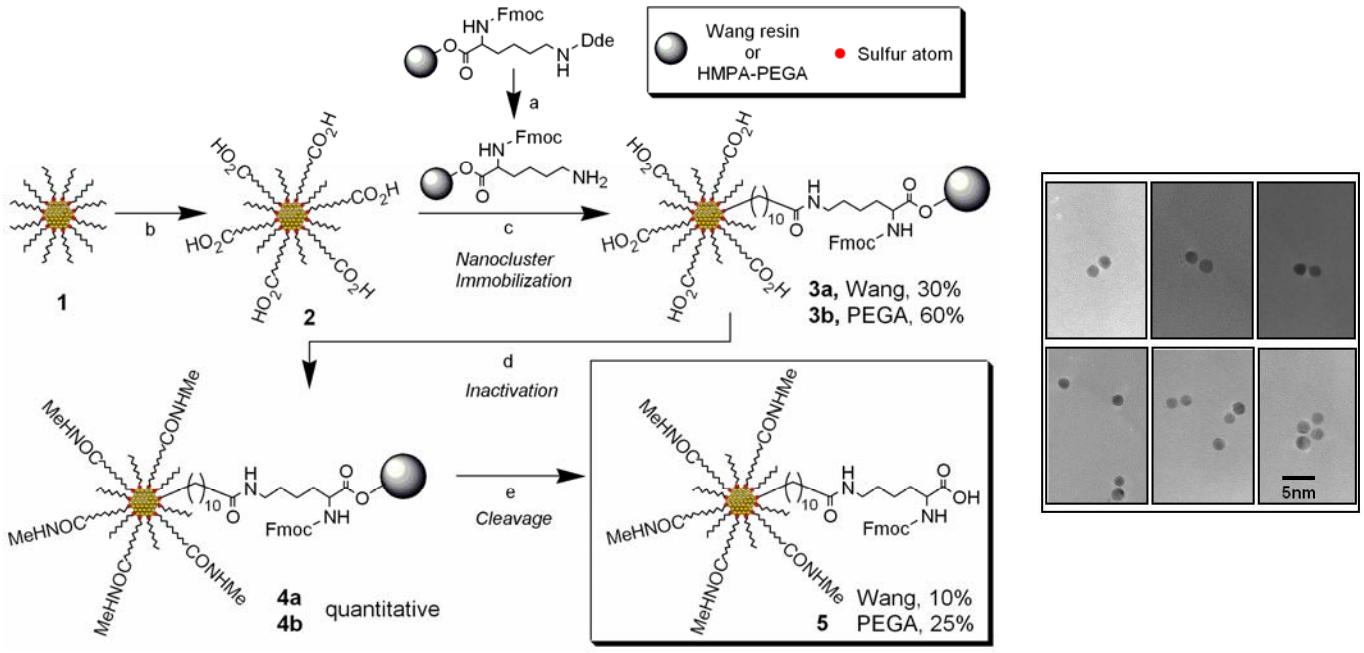

Figure 5. Synthesis and Initial Results for Creating Amino Acid Building Blocks with Electronic Functionality

4. Conclusions and Recommendations

Under this program a general approach towards creating electronically active bio-molecules was outlined. Work on metallic nanoparticle functionalized amino acids in particular was found to be worthy of follow up. If a library of such aminoc acids were created with different functionalities they might form the basis of a new set of building blocks, which could be employed in a peptde synthesizer as a general means of creating peptides with electronic functionality. It is difficult to forsee the full range of applications which might emerge but they should serve to open up new capabilities within molecular biology.

5. References

[1] Hamad-Schifferli, K., Schwartz, J.J., Santos, A.T., Zhang, S, Jacobson, J.M., Remote electronic control of DNA hybridization through inductive coupling to an attached metal nanocrystal antenna, *Nature*, **415**, 2002, pp.152 – 155

[2] Fannin, P.C., Perov, P.A., Charles, S.W., Complex susceptibility measurements of magnetic fluids over the frequency range 50MHz – 18GHz, *J. Phys. D: Appl. Phys*., **32**, 1999, pp.1583-1586.

[3] Chow, B., The Design of a Molecular Assembly Line Based on Biological Molecules, Master's Thesis, Massachusetts Institute of Technology, 2003.

[4] Murray, C.B., Sun, S., Synthesis of monodisperse cobalt nanocrystals and their assembly into magnetic superlattices (invited), *J. Appl. Phys.* **85**, 1999, pp.4325-4330

[5] Sung, K. M., Mosley, D. W., Peelle, B. R., Zhang, S., Jacobson, J. M., Synthesis of Monofunctionalized Gold Nanoparticles by Fmoc Solid-Phase Reactions, *J. AM. CHEM. SOC.* **126**, 2004, pp.5064-5065

J|A|C|S COMMUNICATIONS

Published on Web 03/30/2004

APPENDIX A

Synthesis of Monofunctionalized Gold Nanoparticles by Fmoc Solid-Phase Reactions

Kie-Moon Sung,† David W. Mosley,† Beau R. Peelle,‡,§ Shuguang Zhang,*,‡ and Joseph M. Jacobson*,†

Center for Bits and Atoms, Center for Biomedical Engineering, and Department of Biology and Biological Engineering, Massachusetts Institute of Technology, 77 Massachusetts Avenue, Cambridge, Massachusetts 02139

Received January 23, 2004; E-mail: jacobson@media.mit.edu

Recent progress in nanotechnology has shown highly promising capabilities of nanoparticles (NP) to function as powerful new biological sensory labels and electronic and optical devices.[1] Our laboratory demonstrated that a 1.4-nm gold NP covalently linked to an oligonucleotide is susceptible to radio frequency magnetic fields enabling remote electronic control over the reversible behavior of DNA hybridization.[2] For more elaborate biomolecular controls, multi-NP systems are of interest due to their expected synergistic or interfering ensemble properties with an enhanced complexity. Models for self-assembled hierarchies consisting of nano-building blocks have been suggested,[3] but manipulation with molecular level accuracy is required for precise and reliable fabrication of more complex structures comprising NP building blocks. The protective organic layer of capped NP provides sites for a variety of chemical modifications, yet to date precise control over functional ligand composition has been uncommon and extremely difficult to achieve because reactions heavily rely on unbalanced stoichiometries between small molecules and relatively massive NPs.

We report a versatile monofunctionalization method for gold NPs with L-lysine (Lys). These are potential building blocks for 1D NP peptide chains. Peptides are ubiquitous in biology and afford a wealth of 3D spatial structures and functions, and their exact properties are dictated by the linear order and composition of amino acids. Precise sequential positioning of NPs can be accomplished using peptide synthesis protocols. For this purpose, an amino acid NP building block should meet the following requirements: (a) single amino acid functionality per particle, (b) sufficiently small and uniform core diameters of ~2 nm, a comparable size with major biomolecules, (c) amphiphilic solubility in aqueous and organic media enabling manual or programmed peptide synthesis, and (d) ease of synthesis with minimized effort for purification. Several groups have attempted to string up NPs using rigid polymeric backbones or self-assembly strategies, but generally these methods have been unable to design complex or reliable nanostructures.[4]

To ensure monofuctionalization of NPs, which presents a gigantic challenge in chemical synthesis, we performed a solid-phase reaction. We took advantage of the low-density packing of functional groups present in many solid-phase supports. For example, each functional group on a common PS Wang resin bead possesses a rough volume of at least ~9 nm^3 when suspended in DMF, and thus we hypothesized an NP ≤2 nm can be loaded on the solid phase through a single bond per particle.[5] As shown in Scheme 1, octanethiolate ($CH_3(CH_2)_7S^-$, OT) monolayer-protected gold NPs **1** were taken as robust precursor NPs.[6] Surface modification of **1** by ligand exchange with an excess 11-mercaptoundecanoic acid ($HO_2C(CH_2)_{10}SH$, MUA) in THF afforded reactive amphiphilic NPs **2** in which both ligands are present in approximately equal amounts as reported in the literature.[7]

† Center for Bits and Atoms.
‡ Center for Biomedical Engineering.
§ Department of Biology and Biological Engineering.

Scheme 1. Synthesis of Lys-Monofunctionalized Gold Nanoparticles[a]

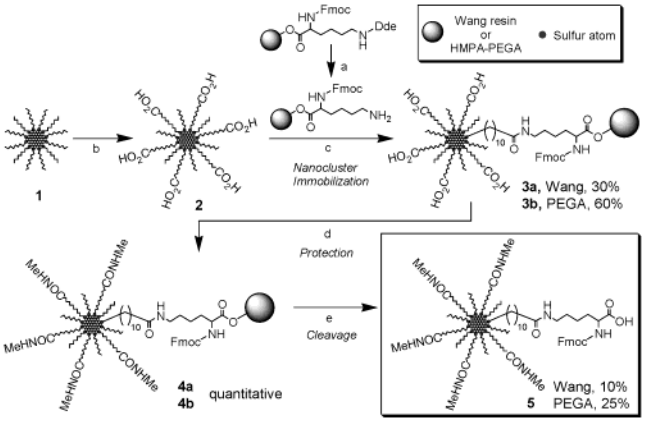

[a] Reagents and conditions: (a) $H_2NNH_2 \cdot H_2O$/DMF (2% v/v), DIPEA/DMF (10% v/v). (b) $HS(CH_2)_{10}CO_2H$ (excess), THF. (c) DIC (excess), DMF/THF (10% v/v) room temperature, 24 h. (d) $MeNH_2$, DIC (excess), DMF/THF, room temperature, 12 h. (e) 60% TFA, 2.5% TIS, 2.5% H_2O, 35% DMF, 24 h.

Core sizes of the NPs **1** and **2** were identified by high-resolution transmission microscopy (HRTEM), and their particle diameters were found to be 2.0 ± 0.3 and 2.1 ± 0.2 nm, respectively. Direct one-pot synthesis of MUA-protected gold NPs was attempted by modifying the method of Ulman and co-workers[8] but was not successful in obtaining monodisperse NPs.

A conventional solid-phase reaction using a 9-fluorenylmethoxycarbonyl (Fmoc) protecting group was then carried out for coupling of NP **2** with Lys. NPs **2** were treated with commercially available Fmoc-Lys(Dde)-Wang PS beads (Dde = 1-(4,4-dimethyl-2,6-dioxocyclohexylidene)ethyl), after the ϵ-amine was deprotected, in the presence of 1,3-diisopropylcarbodiimide (DIC) under the conditions described in Scheme 1. On the basis of the weight gain of the beads, **2** was found to be consumed with ~30% loading level to afford **3a**. High-temperature reaction at 80−100 °C improved NP loading up to ~50%, but the solution color changed to burgundy red within 4 h with the plasmon resonance band at λ_{max} = 520 nm, indicating a significant growth of larger particles of NPs. Features of elemental composition and morphology of **3a** were investigated by scanning electron microscopy (SEM)-assisted energy-dispersive X-ray analysis (EDX) (Supporting Information). A spot profile of nanoparticles immobilized on a resin exhibited the presence of strong signals from carbon and gold atoms, which are the characteristic elemental components of **3a**. To confirm a successful covalent coupling, a resin salt [$(\text{Fmoc-Lys-Wang})^{n+} \cdot \mathbf{2}^{n-}$] was examined by SEM (Supporting Information). In this case, the ionic species cause charging effects, resulting in poorly resolved images, which is quite different from **3**.

Protection of the free carboxyl groups in **3a** was accomplished by a coupling reaction with a slight excess of methylamine to afford

10.1021/ja049578p CCC: $27.50

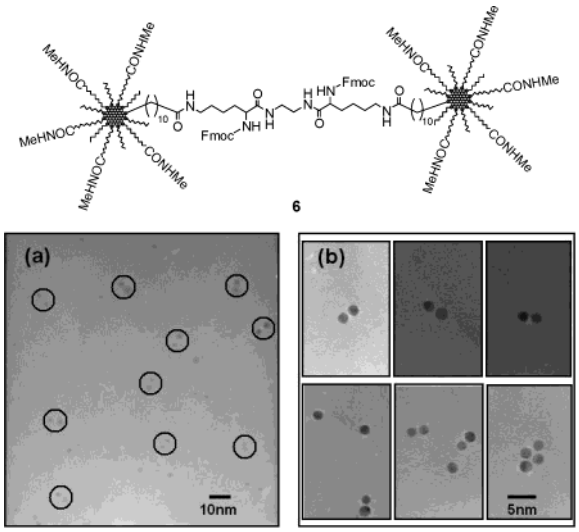

Figure 1. Schematic structure and HRTEM images of gold nanoparticle dimers **6**.

4a in an almost quantitative yield (Scheme 1). Subsequent Lys transfer from Wang resin to the gold nanoparticle was completed by treatment of the bead loaded with **4a** with an acidic cleavage cocktail, 60% trifluoroacetic acid (TFA) in DMF. The cleavage reaction typically took place in 2 h. The first crop of isolated nanoparticles **5** was obtained with ~10% yield from **4a** and with ~3% in overall from **2**.

Due to the low yield of the final product **5** from the reaction with PS Wang resin, we employed an alternative solid support, poly(ethylene glycol)acrylamide copolymer (PEGA)-based resin, which is widely used for on-bead enzyme assays.[9] Resin swelling is key to enhancing substrate permeability to increase loading levels, and PEGA was chosen because it swells approximately four times greater than PS resin in DMF. Fmoc-Lys(Dde)-OH was introduced to PEGA following the dichlorobenzoyl chloride (DBC) method with the use of a tethered linker, 4-hydroxymethylphenoxyacetyl (HMPA). Lys group substitution level on HMPA-PEGA resin was measured to be 0.05 mmol/g in DMF. The remaining procedures for the monofunctionalized gold NPs **5** were similar to those used for the PS Wang resin. Using PEGA beads, we could increase the NP loading level in **3b** and the yield of **5** from **4b** up to 60% and 25%, respectively. Therefore, an HMPA-PEGA support could achieve an overall 15% yield for **5** that is five times higher than that of PS Wang-supported synthesis.

The particle size of **5** remained similar to that of the precursors and was determined to be 2.2 ± 0.3 nm by TEM. An FTIR measurement clearly distinguished **5** from **2** as evidenced by the strong amide I and II peaks at 1700 and 1650 cm^{-1} and ν(N−H) at 3270 cm^{-1} in **5**, respectively (Supporting Information). However, we have been unable to directly detect Lys on NP **5**, because its concentration is very low relative to the majority of the ligands in **5**.

Direct evidence of monofunctionalization is revealed by dimerization of the isolated NPs **5**, which were treated by a slow addition of bridging linker ethylenediamine (excess) in the presence of DIC. Since the carboxyl group of Lys in **5** is the only reactive moiety for the reaction, it is possible to count the number of Lys present in **5** by identifying the associated NPs. As anticipated, TEM images in Figure 1a demonstrate that the dimeric species **6** are dominant and that 55−60% of particles on the TEM grid are found to undergo dimerization, reflecting that at least 55% NPs are monofunctionalized. The interparticle distance is 1.8 ± 0.5 nm, which is less than the estimated 4.8-nm length for a fully extended bridge. This could indicate that the bridging ligand is coiled to the side and that the ligand sphere of the particles may be interdigitated. Interestingly, there appears to be no significant difference in the dimerization features originating from the use of different solid supports. NPs **5** from either PS Wang resin or PEGA gave almost identical particle size distribution and dimerization efficacy of ~60% toward **6**. Some monomers and higher-order clusters were observed (Figure 1b), suggesting that some particles may be functionalized by multiple Lys or may not have reacted in the dimerization reaction. It is uncertain whether these monomers and higher-order clusters contain significant amounts of monofunctionalized NPs, and the actual yield for monofunctionalized ones may be higher if a more accurate assay is found. This is a highly selective method for monofunctionalization of NPs compared to the routine stoichiometric reactions. For instance, Feldheim and co-workers have reported a stoichiometric assembly of gold NPs into dimers using a rigid bridging linker, and their efficiency in dimer formation was as high as ~47%.[10]

In summary, we have synthesized ~2-nm sized Lys-monofunctionalized gold NPs **5** in a highly selective manner by solid-phase reaction using PS Wang resin or HMPA-PEGA. Productivity and reaction efficiency are highly dependent on the swelling properties of the solid support, which is not common in solid-phase organic synthesis. We are currently working to employ these NP building blocks in a peptide synthesis strategy.

Acknowledgment. This work was supported by grants from DARPA Biocomputing, DARPA/AFO NURI/AFO, and Things That Think Consortium of MIT Media Lab. We thank Michael Frongello and Vikas Anant for the electron microscopy measurements.

Supporting Information Available: Experimental details for the synthesis of the gold nanoparticles (PDF). This material is available free of charge via the Internet at http://pubs.acs.org.

References

(1) (a) Bruchez, M., Jr.; Moronne, M.; Gin, P.; Weiss, S.; Alivisatos, A. P. *Science* **1998**, *281*, 2013−2016. (b) Xiao, Y.; Patolsky, F.; Katz, E.; Hainfeld, J. F.; Willner, I. *Science* **2003**, *299*, 1877−1881. (c) Storhoff, J. J.; Mirkin, C. A. *Chem. Rev.* **1999**, *99*, 1849−1862 and references therein. (d) Thanh, N. T. K.; Rosenzweig, Z. *Anal. Chem.* **2002**, *74*, 1624−1628. (e) Maxwell, D. J.; Taylor, J. R.; Nie, S. *J. Am. Chem. Soc.* **2002**, *124*, 9606−9612. (f) Klein, D. L.; Roth, R.; Lim, A. K. L.; Alivisatos, A. P.; McEuen, P. L. *Nature* **1997**, *389*, 699−701. (g) Otsuka, H.; Akiyama, Y.; Nagasaki, Y.; Kataoka, K. *J. Am. Chem. Soc.* **2001**, *123*, 8226−8230.

(2) Hamad-Schifferli, K.; Schwartz, J. J.; Santos, A. T.; Zhang, S.; Jacobson, J. M. *Nature* **2002**, *415*, 152−155.

(3) Zhang, Z.; Horsch, M.; Lamm, M. H.; Glotzer, S. C. *Nano Lett.* **2003**, *3*, 1341−1346

(4) (a) Fullam, S.; Cottell, D.; Rensmo, H.; Fitzmaurice, D. *Adv. Mater.* **2000**, *12*, 1430−1432. (b) Stevenson, K. A.; Muralidharan, G.; Maya, L.; Wells, J. C.; Barhen, J.; Thundat, T. *J. Nanosci. Nanotechnol.* **2002**, *2*, 397−404. (c) Jiang, K.; Eitan, A.; Schadler, L. S.; Ajayan, P. M.; Siegel, R. W.; Grobert, N.; Mayne, M.; Reyes-Reyes, M.; Terrones, H.; Terrones, M. *Nano Lett.* **2003**, *3*, 275−277. (d) Marinakos, S. M.; Brousseau, L. C., III; Jones, A.; Feldheim, D. L. *Chem. Mater.* **1998**, *10*, 1214−1219. (e) Liao, J. H.; Chen, K. J.; Xu, L. N.; Ge, C. W.; Wang, J.; Huang, L.; Gu, N. *Appl. Phys. A* **2003**, *76*, 541−543. (f) Liao, J.; Zhang, Y.; Xu, L.; Ge, C.; Liu, J.; Gu, N. *Colloids Surf., A* **2003**, *223*, 177−183.

(5) Values were estimated by calculation based on data for the functional group substitution level and resin swelling volume (1% DVB-cross-linked, 100−200 mesh, 0.54 mmol/g substitution level, swelling volume 3 mL/g in DMF), and solid matrix volume and porosity were not taken into account.

(6) Hostetler, M. J.; Wingate, J. E.; Zhong, C.-J.; Harris, J. E.; Vachet, R. W.; Clark, M. R.; Londono, J. D.; Green, S. J.; Stokes, J. J.; Wignall, G. D.; Glish, G. L.; Porter, M. D.; Evans, N. D.; Murray, R. W. *Langmuir* **1998**, *14*, 17−30.

(7) Simard, J.; Briggs, C.; Boal, A. K.; Rotello, V. M. *Chem. Commun.* **2000**, 1943−1944.

(8) Yee, C. K.; Jordan, R.; Ulman, A.; White, H.; King, A.; Rafailovich, M.; Sokolov, J. *Langmuir* **1999**, *15*, 3486-3491.

(9) Meldal, M. *Biopolymers* **2002**, *66*, 93−100.

(10) (a) Novak, J. P.; Brousseau, L. C., III; Vance, F. W.; Johnson, R. C.; Lemon, B. I.; Hupp, J. T.; Feldheim, D. L. *J. Am. Chem. Soc.* **2000**, *122*, 12029−12030. (b) Novak, J. P.; Feldheim, D. L. *J. Am. Chem. Soc.* **2000**, *122*, 3979−1980. (c) Brousseau, L. C., III; Novak, J. P.; Marinakos, S. M.; Feldheim, D. L. *Adv. Mater.* **1999**, *11*, 447−449.

JA049578P

magnetization process can be considered as being reversible in temperature. From the magnetization curve at 5 K, the saturation magnetization was determined as 3.9 μ_B per formula unit. This high magnetization originates from the parallel alignment of the Mn and Fe moments, though the moments of Mn are much larger than those of Fe (ref. 12). Variation of the Mn/Fe ratio may also be used to further improve the MCE.

The magnetic entropy changes, ΔS_m, are calculated from magnetization data by means of the equation

$$\Delta S_m(T,B) = S_m(T,B) - S_m(T,0) = \int_0^B \left(\frac{\partial M}{\partial T}\right)_{B'} \mathrm{d}B'$$

which is based on a Maxwell relation. The results are shown in Fig. 3. The calculated maximum values of the magnetic entropy changes are 14.5 J kg^{-1} K^{-1} and 18 J kg^{-1} K^{-1} for field changes from 0 to 2 T and 0 to 5 T, respectively. The maximum magnetic entropy in 3*d* materials depends on the spin moment *S*. Because there are two magnetic ions per formula unit, we have $S_m = 2R\ln(2S + 1)$, where *R* is the universal gas constant. From the saturation magnetic moment, we estimate the average *S* value of the magnetic ions to be 1, thus $S_m = 18.3$ J mol^{-1} K^{-1} = 117 J kg^{-1} K^{-1}, which is about 6 times larger than the value obtained from the magnetization measurements. For comparison, the magnetic entropy change of the compound $Gd_5Ge_2Si_2$ and Gd is also shown in Fig. 3. It is evident that the MCE in $MnFeP_{1-x}As_x$ compounds is comparable with that of $Gd_5Ge_2Si_2$, though the Gd compound has a larger magnetic moment at 5 K. The origin of the large magnetic entropy change is in the comparatively high 3*d* moments and in the rapid change of magnetization in the field-induced magnetic phase transition. In rare-earth materials, the magnetic moment fully develops only at low temperatures, and therefore the entropy change near room temperature is only a fraction of the potential value. In 3*d* compounds, the strong magneto-crystalline coupling results in competing intra- and inter-atomic interactions, and leads to a modification of metal–metal distances which may change the iron and manganese magnetic moments and favour spin ordering.

The excellent magnetocaloric features of the compound $MnFeP_{0.45}As_{0.55}$, in addition to the very low material costs, make it an attractive candidate material for a commercial magnetic refrigerator. □

Received 30 July; accepted 6 November 2001.

1. Glanz, J. Making a bigger chill with magnets. *Science* **279,** 2045 (1998).
2. Pecharsky, V. K. & Gschneidner, K. A. Jr Giant magnetocaloric effect in $Gd_5(Si_2Ge_2)$. *Phys. Rev. Lett.* **78,** 4494–4497 (1997).
3. Gschneidner, K. A. Jr *et al.* Recent developments in magnetic refrigeration. *Mater. Sci. Forum* **315–317,** 69–76 (1999).
4. Zimm, C. *et al.* Description and performance of a near-room temperature magnetic refrigerator. *Adv. Cryogen. Eng.* **43,** 1759–1766 (1998).
5. Tishin, A. M. in *Handbook of Magnetic Materials* Vol. 12 (ed. Buschow, K. H. J.) 395–524 (North Holland, Amsterdam, 1999).
6. Choe, W. *et al.* Making and breaking covalent bonds across the magnetic transition in the giant magnetocaloric material $Gd_5(Si_2Ge_2)$. *Phys. Rev. Lett.* **84,** 4617–4620 (2000).
7. Giguere, A. *et al.* Direct measurement of the "giant" adiabatic temperature change in $Gd_5(Si_2Ge_2)$. *Phys. Rev. Lett.* **83,** 2262–2265 (1999).
8. Morellon, L. *et al.* Nature of the first-order antiferromagnetic-ferromagnetic transition in the Ge-rich magnetocaloric compounds $Gd_5(Si_xGe_{1-x})_4$. *Phys. Rev. B* **62,** 1022–1026 (2000).
9. Pytlik, L. & Zieba, A. Magnetic phase diagram of MnAs. *J. Magn. Magn. Mater.* **51,** 199–210 (1985).
10. Zach, R., Guillot, M. & Fruchart, R. The influence of high magnetic fields on the first order magneto-elastic transition in $MnFe(P_{1-y}As_y)$ systems. *J. Magn. Magn. Mater.* **89,** 221–228 (1990).
11. Bacmann, M. *et al.* Magnetoelastic transition and antiferro-ferromagnetic ordering in the system $MnFeP_{1-y}As_y$. *J. Magn. Magn. Mater.* **134,** 59–67 (1994).
12. Beckman, O. & Lundgren, L. in *Handbook of Magnetic Materials* (ed. Buschow, K. H. J.) Vol. 6, 181–287 (North Holland, Amsterdam, 1991).

Acknowledgements

We thank A.J. Riemersma for preparation of graphs. Part of this work was performed within the scientific exchange program between the Netherlands and China. This work was financially supported by the Dutch Technology Foundation STW.

Correspondence and requests for materials should be addressed to E.B. (e-mail: bruck@wins.uva.nl).

12

Remote electronic control of DNA hybridization through inductive coupling to an attached metal nanocrystal antenna

Kimberly Hamad-Schifferli*, John J. Schwartz†, Aaron T. Santos*, Shuguang Zhang‡ & Joseph M. Jacobson*

** The Media Laboratory and the ‡Center for Biomedical Engineering, Massachusetts Institute of Technology, 77 Massachusetts Ave., Cambridge, Massachusetts 02139, USA*
† Engeneos, 40 Bear Hill Road, Waltham, Massachusetts 02451, USA

Increasingly detailed structural[1] and dynamic[2,3] studies are highlighting the precision with which biomolecules execute often complex tasks at the molecular scale. The efficiency and versatility of these processes have inspired many attempts to mimic or harness them. To date, biomolecules have been used to perform computational operations[4] and actuation[5], to construct artificial transcriptional loops that behave like simple circuit elements[6,7] and to direct the assembly of nanocrystals[8]. Further development of these approaches requires new tools for the physical and chemical manipulation of biological systems. Biomolecular activity has been triggered optically through the use of chromophores[9–14], but direct electronic control over biomolecular 'machinery' in a specific and fully reversible manner has not yet been achieved. Here we demonstrate remote electronic control over the hybridization behaviour of DNA molecules, by inductive coupling of a radio-frequency magnetic field to a metal nanocrystal covalently linked to DNA[15]. Inductive coupling to the nanocrystal increases the local temperature of the bound DNA, thereby inducing denaturation while leaving surrounding molecules relatively unaffected. Moreover, because dissolved biomolecules dissipate heat in less than 50 picoseconds (ref. 16), the switching is fully reversible. Inductive heating of macroscopic samples is widely used[17–19], but the present approach should allow extension of this concept to the control of hybridization and thus of a broad range of biological functions on the molecular scale.

Inductive coupling is the transfer of energy between circuits. If the secondary circuit has finite impedance, eddy currents are produced which are converted to heat by the Joule effect[17]. Heating a conductor by placing it in an alternating magnetic field is generally used to heat macroscopic samples. Here we apply it to metallic nanocrystals (diameter 1.4 nm) in solution. Induction heating is accompanied by a skin-depth effect, resulting from partial cancellation of the magnetic fields. Consequently, most of the power absorbed by the conductor is concentrated in a depth d_0, given by:

$$d_0 = \frac{1}{2\pi}\sqrt{\frac{\rho 10^7}{\mu_r \mu_0 f}} \quad (1)$$

where μ_r is magnetic permeability, μ_0 is the permeability of free space, ρ is the material resistivity, and f is the frequency of the alternating magnetic field. The power density P is given by:

$$P = 4\pi H_c^2 \mu_0 \mu_r f F \frac{d_0}{d} \quad (2)$$

where d is the sample diameter, H_e is the magnetic field strength, and F is a transmission factor that has a sigmoidal dependence on d/d_0. Optimal power absorption and heating occur when $d/d_0 = 3.5$. To optimally heat by induction a gold nanocrystal with $d = 1.4$ nm, $f = 49$ GHz (radio frequency range) is required[17,18]. Here we use

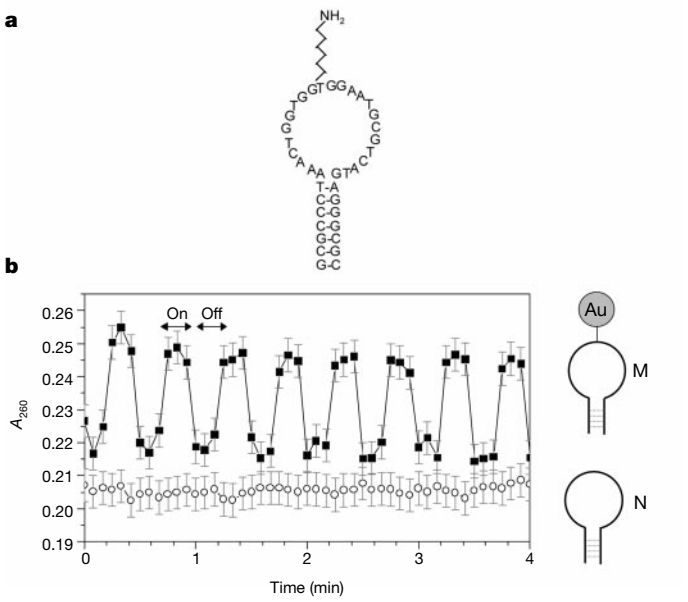

Figure 1 Inductive coupling to nanocrystals linked to DNA and evidence of dehybridization. **a**, Sequence of the hairpin molecule, M. The molecule is self-complementary at the ends for 7 bases, with a primary amine in the loop to which a 1.4-nm gold nanocrystal is covalently linked. **b**, Absorbance at 260 nm (A_{260}) of a solution of M in RFMF (squares). Arrows indicate when the RFMF is on/off. Circles, response of N (no nanocrystals) in RFMF. Gold nanocrystals also show an absorbance increase under RFMF, qualitatively attributed to the change in the optical absorption due to eddy currents. However, the absorbance increases nearly uniformly over 200–300 nm with RFMF and is small relative to the oligo change in absorbance. To obtain the data shown here, the nanocrystal contribution was subtracted (see Supplementary Information for details). M with a fluorophore/quencher pair on the ends shows fluorescence increasing reversibly with RFMF (not shown), confirming dehybridization.

f = 1 GHz, which results in a skin depth larger than the particle so that the entire particle is heated. We note that additional mechanisms, including induced dipole torque on the nanoparticle which increases the kinetic energy of the nanoparticles, may be important at these length scales. The physics of heating nanometre particles has not been explored previously, and will be the subject of future investigations. There are numerous examples of the heating of magnetic particles by a magnetic field for the treatment of tumours through macroscopic tissue heating[19]. However, we emphasize that the (magnetite) particles in such cases are several orders of magnitude larger in volume than the particles used in our investigation, and are not interfaced to individual molecules.

In order to demonstrate reversible electronic control, we have constructed a DNA hairpin-loop oligonucleotide covalently linked to a nanometre scale antenna. 38-nucleotide hairpin-loop DNA which is self-complementary at each end for 7 bases[20] (Fig. 1a) was covalently linked to a 1.4-nm gold nanocrystal by a primary amine appended to a single base[21–24]. Because of the loop constraint, the DNA rehybridizes on a timescale comparable to dehybridization[25]. The dehybridization was monitored by the hyperchromicity of DNA, measured by optical absorbance at 260 nm (A_{260})[26]. A solution of the nanocrystal-linked oligonucleotides (referred to as M) was put into a radio-frequency magnetic field (RFMF) with f = 1 GHz. A_{260} was monitored in an ultraviolet–visible spectro-

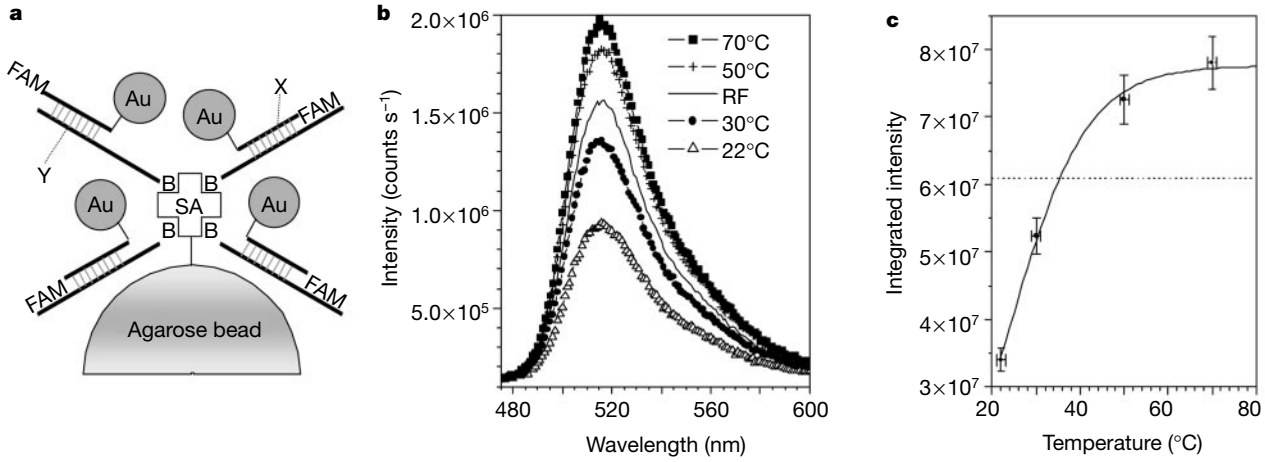

Figure 2 Determination of effective temperature from inductive coupling to a gold nanocrystal linked to DNA. **a**, The two-phase system. X is a 12-nucleotide DNA molecule covalently labelled with a gold nanocrystal on its 3′ end and the fluorophore FAM on its 5′ end. Its complementary strand Y has biotin (B) on the 5′ end, which was captured onto agarose beads with streptavidin (SA) on the surface. Once X dehybridizes from Y it can diffuse into the supernatant. **b**, Supernatant fluorescence spectra. Each sample is subject to a fixed temperature (22 °C, 30 °C, 50 °C, 70 °C) or RFMF (solid line). **c**, Integrated peak intensity of the supernatant fluorescence spectra shown in **b** (circles) and a sigmoidal fit (solid line), and the intensity of the sample exposed to RFMF (dotted line). Extrapolation of RFMF sample intensity results in an effective temperature of 35 °C for X.

photometer as the RFMF was pulsed at 15-s intervals (Fig. 1b). As the RFMF was switched on, A_{260} increased from 0.22 to 0.25, indicating that M dehybridized with the RFMF (squares in Fig. 1b). When the RFMF was switched off, A_{260} returned to its original value. Cycling through the on and off states was repeatable. The on/off ratio of A_{260} is 1.09, consistent with calculated absorption coefficients for this sequence hybridizing and dehybridizing 7 bases. Control solutions with DNA only (that is, not linked to gold nanocrystals), referred to as N, resulted in no change in the absorbance with RFMF (circles in Fig. 1b). This shows that inductive coupling to a covalently bound metal nanocrystal can reversibly dehybridize DNA on a timescale of at most several seconds.

To determine the effective temperature that inductive coupling to the nanocrystal produces locally, we designed a two-phase system in which DNA is dehybridized from a solid support into solution (Fig. 2a). X is a 12-nucleotide DNA molecule with a nanocrystal on the 3′ end and a fluorophore (FAM) on the 5′ end (see Methods). It was hybridized to its complement Y, which was immobilized onto 100-μm streptavidin-coated agarose beads comprising the solid phase. As X dehybridizes from Y, it diffuses into the supernatant. The amount of dehybridization is proportional to the amount of X in the supernatant, which was measured by fluorescence spectroscopy. One aliquot of the sample was exposed to the RFMF and its supernatant removed. Its fluorescence spectrum was compared to supernatants of aliquots thermally heated at specific temperatures. The intensity of the supernatant fluorescence spectra (Fig. 2b) increases with temperature, indicative of increased amounts of X dehybridized. The sample exposed to RFMF has intensity (solid line) in between the 30 °C and 50 °C samples. The integrated peak intensity of the spectra (Fig. 2c) as a function of temperature (squares) can be fitted to a sigmoidal (solid line), corresponding to a thermal denaturation curve. The intensity of the RFMF sample (dashed line) extrapolates to 35 °C, indicating that the effective temperature increase on X produced by the RFMF is +13 °C. This change in temperature is sufficient for control of many biological processes.

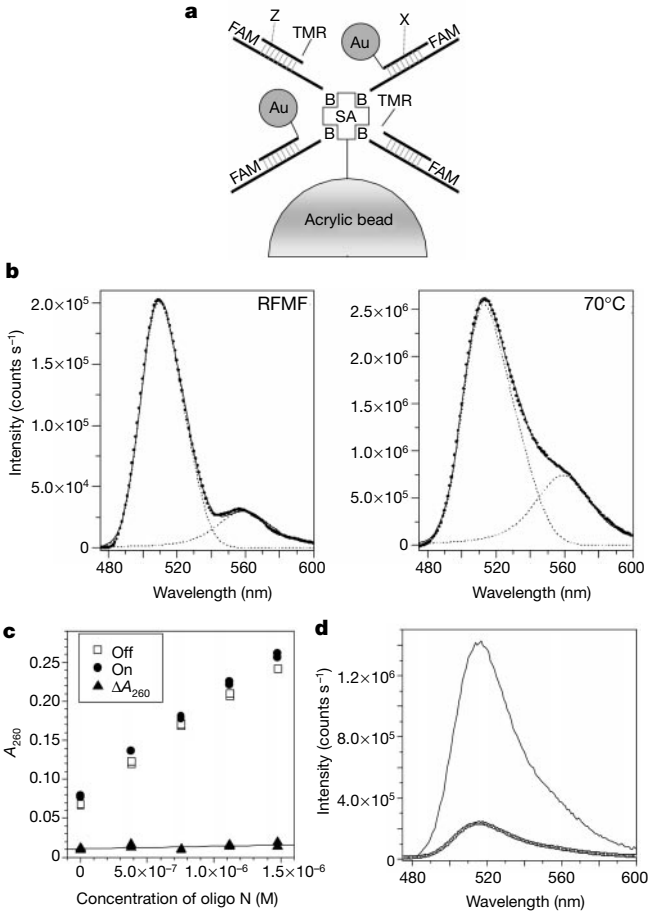

Figure 3 Testing selectivity. **a**, Two-phase system. Z is identical to X but has the fluorophore TMR on the 3′ end (λ_{max} = 563 nm). The beads have both X-Y and Z-Y hybrids. **b**, Difference fluorescence spectra (dots) (after dehybridization by heat/RFMF minus before dehybridization) scaled to same height. Shown are individual fluorescence peak fits (dashed lines) and composite fits (solid lines). When fitting the experimental data obtained upon RFMF and heat exposure, two spectral peaks centred at 516 nm and 563 nm and having full-widths at half-maximum of 31 nm and 38 nm, respectively, were used in each case. Sample exposed to RFMF (left) and to 70 °C (right). **c**, A_{260} of M and N mixture with RFMF on (circles) and off (squares), ΔA_{260} (triangles), and fit (line) as a function of N concentration. The concentration of M is 1.12×10^{-7} M while N ranges from 0 to 1.4×10^{-6} M. Based on concentrations the estimated density is ~1 molecule per 10^6 nm^3, an upper limit on intermolecular separation as it does not account for diffusion. **d**, Spectra of supernatants with one (dots) or two (line) RFMF dehybridizations normalized to the intensity of the 70 °C aliquot for each sample.

One important property is the ability to address molecules with a nanocrystal while having a lesser effect on molecules not bound to a nanocrystal. If induction heating of the nanocrystal is sufficiently spatially localized, it will afford selectivity. We used a two-phase system in which X was mixed with Z, identical in sequence to X but instead has TMR (see Methods) on the 3′ end (Fig. 3a). TMR emits at a wavelength distinct from FAM (λ_{max} = 563 nm). The two-phase system comprises tetrameric avidin acrylic beads with both X-Y and Z-Y hybrids on the surface in approximately equimolar amounts. One sample was exposed to RFMF, and the supernatant was compared to a thermally heated sample (70 °C) by fluorescence. The difference of the spectrum before and after dehybridization for the 70 °C sample (Fig. 3b, right) has peaks at 515 nm and 563 nm, indicating dehybridization of both X and Z. The RFMF sample (Fig. 3b, left) shows intensity at 515 nm due to dehybridized X but negligible intensity at 563 nm, which indicates selectivity: Z is relatively unaffected by induction heating of X in its proximity. Quantification of the spectra yields ~80% X for the RFMF sample and ~55% for the 70 °C sample. The slight amount of Z dehybridized in the RFMF sample is presumably due to the proximity of the molecules associated with tetrameric avidin (intermolecular separation is expected to be ≥ 10 nm).

RFMF experiments on solutions of mixtures of M and N also illustrate selective heating. Figure 3c shows A_{260} with RFMF on and off for a fixed concentration of M as N was added. Values of A_{260} for the on and off states increase linearly, but the difference (ΔA_{260}) remains constant. Samples of increasing concentration of M show ΔA_{260} increasing with concentration (not shown). These experiments indicate that induction heating of the nanocrystal on M is sufficiently localized that N is unaffected. Another indication of selectivity of RFMF dehybridization is evident in the purification of gold-linked X from unlabelled X, where the fraction of gold-linked oligonucleotides increases with successive RFMF dehybridizations. Figure 3d shows the fluorescence spectra of a sample before and after RFMF purification. A sample of partially labelled X is RFMF dehybridized and compared to a 70 °C aliquot, which effectively provides the total number of X in the system (dots). If the RFMF supernatant is rehybridized to Y and RFMF dehybridized a second time, its intensity is higher relative to the 70 °C aliquot (lines). The percentage of molecules dehybridized by RFMF increases after purification, suggesting the RFMF preferentially dehybridizes X linked with nanocrystals. If RFMF dehybridization were non-selective, this percentage would be the same for both samples. These experiments show that induction heating of the nanocrystal is localized such that surrounding molecules are not substantially affected.

Manipulation of DNA by itself is useful, as it has potential as an

actuator[5] and performing computations[27]. Because nanocrystals can be readily attached to proteins, switching more complex processes—such as enzymatic activity (S.Z., J. Shi, M. Jura, K.H.-S., J.J.S. and J.M.J, manuscript in preparation), biomolecular assembly, gene regulation, and protein function—might be possible. Due to the spatial localization of denaturation, it might be possible to control portions of proteins or nucleic acids while the rest of the molecule and neighbouring species would remain relatively unaffected. Control of dehybridization of antisense oligos in transcription[28] would permit reversible control of the production of specific messenger RNA. Because the addressing is not optical, this technology could be useful in highly scattering media. □

Methods

Linking gold nanocrystals to DNA hairpin-loop molecules

DNA oligonucleotides were synthesized via solid-phase synthesis (Research Genetics) with addition of internal amines, terminal biotin, or fluorophores. DNA hairpin-loop oligonucleotides of the type used to make M ('molecular beacons[20]') have a thymine in the loop region which was modified on the 5 position of the base with a C6 primary amine, to which a nanocrystal was covalently linked. 1.4-nm uncharged gold nanocrystals functionalized with a single sulpho *N*-hydroxy-succinimide (NHS) ester[29] (Nanoprobes) were incubated with the oligonucleotide in the manufacturer's buffer at room temperature for 1 h, resulting in a covalent bond between the nanocrystal and oligonucleotide[30]. Nanocrystals were in molar excess (>10 ×). Excess nanocrystals were removed by 70% ethanol precipitation on ice and repeated washes. The nanocrystals are soluble in ethanol, but the DNA or species attached to it precipitates. Gel electrophoresis is effective in separating nanocrystals from DNA-labelled gold nanocrystals, but for short DNA the mobility shift is expected to be too small to resolve the two species[24]. The concentration of M and N is 1×10^{-6} M in 1X PBS (1X PBS = 1 mM KH_2PO_4, 10 mM Na_2HPO_4, 137 mM NaCl, 2.7 mM KCl).

RFMF

Alternating magnetic fields were generated by applying an alternating current to a coil with 35 turns and a cross section of ~1 cm^2. Coils were wrapped around a plastic cuvette/tube holder with open structures to maximize light passage. Currents with $f = 1$ GHz were obtained using an RF signal generator (Hewlett Packard 8648C) with an output of 1 mW in conjunction with a linear amplifier. The ultimate output power range used was 0.4–4 W, though these are upper limits to the exact power inside the coil due to losses from set-up architecture (10% input power estimated to be transferred to coil). DNA hairpin samples (volume 200 μl) were in a 3 mm × 3 mm quartz cuvette inside the coil. The two-phase samples were in 250-μl plastic tubes (supernatant volume 165 μl, solid phase volume 60 μl) put into the coil in a water bath. The power used for the experiments shown in Figs 1 and 2 was 4 W, and 1 W for those in Fig. 3.

Spectroscopy

UV–visible spectra were taken on a DU530 Beckman spectrophotometer with time resolution limited to 5-s steps. Fluorescence spectra was taken on a Spex Fluoromax fluorometer with 1-nm steps, 0.1-s integration time, entrance/exit slits 1–5 nm, $\lambda_{excitation}$ = 450 nm. Signal was averaged multiple times (≤10). Fluorescence peak areas were quantified by Voigt lineshape deconvolution using a commercial program (Peakfit, SPSS). Figure 3b fits had the same parameters for peak positions and widths for both spectra.

Two-phase system

Molecule X is a 12-nucleotide DNA that has a 6-carboxyfluorescein (FAM, λ_{max} = 516 nm) on the 5′ end and a C6 primary amine on the 3′ end (T_m = 40 °C). It was labelled with the nanocrystal as described above. Molecule Y is a 68-nucleotide DNA complementary to X, and has a biotin on the 5′ end. X and Y were hybridized, and the X-Y hybrid was incubated with streptavidin agarose beads (Sigma-Aldrich) with $<d>$ = 100 μm to allow the biotin on Y to bind to streptavidin. Samples were washed several times with 1X PBS to remove free gold. This biotin–streptavidin reaction ($K_d = 10^{-15}$ M) is robust for the temperatures used here[30]. Tests in which bead-bound Y was heated to 85 °C showed no presence of oligonucleotide in the supernatant, confirming the biotin–streptavidin interaction was intact.

In the construction of the two-phase system (Fig. 2), X was purified from unlabelled oligonucleotides by exposing bead-immobilized X-Y to RFMF. Oligonucleotides not linked to a nanocrystal had no response to RFMF and thus remain hybridized to Y. This is another alternative to purification by gel electrophoresis[24]. Purified X was hybridized to Y, then exposed to streptavidin agarose beads to immobilize X-Y. After multiple washes with 1X PBS, buffer was added to the beads to serve as the liquid phase. Samples were exposed to RFMF or heated conventionally at a specific temperature for 5 min. Following heating or exposure to the RFMF, the supernatants were separated from the beads and then measured by fluorescence spectroscopy. All fluorescence spectra were taken under identical conditions (temperature, spectrometer parameters).

Mixed two-phase system

Oligonucleotide Z was identical in sequence to X but was labelled on the 3′ end with NHS-tetramethylrhodamine (TMR, Molecular Probes). Attachment of the TMR to the primary amine on Z was achieved by incubating the molecules together in sodium bicarbonate solutions (1 h, room temperature) in the dark to prevent photobleaching (manufacturer directions). Oligonucleotide Z was hybridized to Y, mixed in solution with X-Y, then incubated with tetrameric avidin acrylic beads (Sigma-Aldrich) as described above. Free molecules were removed with multiple washes of 1X PBS. The sample is equimolar in X to Z on the beads. The surface density of the monomeric avidin on the beads is ~1 molecule per nm^2.

Received 12 July; accepted 16 November 2001.

1. Ban, N., Nissen, P., Hansen, J., Moore, P. B. & Steitz, T. A. The complete atomic structure of the large ribosomal subunit at 2.4 Å resolution. *Science* **289,** 905–920 (2000).
2. Deniz, A. A. *et al.* Single-molecule protein folding: Diffusion fluorescence resonance energy transfer studies of the denaturation of chymotrypsin inhibitor 2. *Proc. Natl Acad. Sci. USA* **97,** 5179–5184 (2000).
3. Davenport, R., Wuite, G., Landick, R. & Bustamante, C. Single-molecule study of transcriptional pausing and arrest by *E. coli* RNA polymerase. *Science* **287,** 2497–2500 (2000).
4. Winfree, E., Liu, F., Wenzler, L. & Seeman, N. Design and self-assembly of two-dimensional DNA crystals. *Nature* **394,** 539–44 (1998).
5. Yurke, B. *et al.* A DNA-fuelled molecular machine made of DNA. *Nature* **406,** 605–608 (2000).
6. McAdams, H. H. & Arkin, A. Gene regulation: towards a circuit engineering discipline. *Curr. Biol.* **10,** R318–R320 (2000).
7. Elowitz, M. B. & Leibler, S. A synthetic oscillatory network of transcriptional regulators. *Nature* **403,** 335–338 (2000).
8. Whaley, S. R., English, D. S., Hu, E. L., Barbara, P. F. & Belcher, A. M. Selection of peptides with semiconductor binding specificity for directed nanocrystal assembly. *Nature* **405,** 665–668 (2000).
9. Telford, J. R., Wittung-Stafshede, P., Gray, H. B. & Winkler, J. R. Protein folding triggered by electron transfer. *Acc. Chem. Res.* **31,** 755–763 (1998).
10. Monroe, W. T., McQuain, M. M., Chang, M. S., Alexander, J. S. & Haselton, F. R. Targeting expression with light using caged DNA. *J. Biol. Chem.* **274,** 20895–20900 (1999).
11. Asanuma, H., Yoshida, T., Ito, T. & Komiyama, M. Photo-responsive oligonucleotides carrying azobenzene at the 2'-position of uridine. *Tetrahedr. Lett.* **40,** 7995–7998 (1999).
12. Liu, D., Karanicolas, J., Yu, C., Zhang, Z. & Woolley, G. A. Site-specific incorporation of photo-isomerizable azobenzene groups into Ribonuclease S. *Bioorg. Med. Chem. Lett.* **7,** 2677–2680 (1997).
13. Haupts, U., Tittor, J. & Oesterhelt, D. Closing in on bacteriorhodopsin: progress in understanding the molecule. *Annu. Rev. Biophys. Biomol. Struct.* **28,** 367–99 (1999).
14. Ashkenazi, G., Ripoll, D. R., Lotan, N. & Scheraga, H. A. A molecular switch for biochemical logic gates: Conformational studies. *Biosens. Bioelectron.* **12,** 85–95 (1997).
15. Hamad-Schifferli, K., Schwartz, J. J., Santos, A. T., Zhang, S. & Jacobson, J. M. in *Mater. Res. Soc. Proc.* (eds Hahn, H. W., Feldheim, D. L., Kubiak, C. P., Tannenbaum, R. & Siegel, R. W.) Y8.43 (MRS, San Francisco, 2001).
16. Lian, T., Locke, B., Kholodenko, Y. & Hochstrasser, R. M. Energy flow solute to solvent probed by femtosecond IR spectroscopy: malachite green and heme protein solutions. *J. Phys. Chem.* **98,** 11648–11656 (1994).
17. Orfeuil, M. *Electric Process Heating: Technologies/ Equipment/ Applications* (Battelle Press, Columbus, Ohio, 1987).
18. Zinn, S. & Semiatin, S. L. *Elements of Induction Heating, Design Control, and Applications* (ASM International, Materials Park, Ohio, 1988).
19. Hergt, R. *et al.* Physical limits of hyperthermia using magnetite fine particles. *IEEE Trans. Magn.* **34,** 3745–3754 (1998).
20. Bonnet, G., Tyagi, S., Libchaber, A. & Kramer, F. R. Thermodynamic basis of the enhanced specificity of structured DNA probes. *Proc. Natl Acad. Sci. USA* **96,** 6171–6176 (1999).
21. Taton, A. T., Mirkin, C. A. & Letsinger, R. L. Scanometric DNA array detection with nanoparticle probes. *Science* **289,** 1757–1760 (2000).
22. Loweth, C. J., Caldwell, W. B., Peng, X., Alivisatos, A. P. & Schultz, P. G. DNA-based assembly of gold nanocrystals. *Angew. Chem. Int. Edn Engl.* **38,** 1808–1812 (1999).
23. Mattoussi, H. *et al.* Self-assembly of CdSe-ZnS quantum dot bioconjugates using an engineered recombinant protein. *J. Am. Chem. Soc.* **122,** 12142–12150 (2000).
24. Zanchet, D., Micheel, C. M., Parak, W. J., Gerion, D. & Alivisatos, A. P. Electrophoretic isolation of discrete Au nanocrystal/DNA conjugates. *Nanoletters* **1,** 32–35 (2001).
25. Bonnet, G., Krichevsky, O. & Libchaber, A. Kinetics of conformational fluctuations in DNA hairpin-loops. *Proc. Natl Acad. Sci. USA* **95,** 8602–8606 (1998).
26. Cantor, C. R. & Schimmel, P. *Biophysical Chemistry* (Freeman, San Francisco, 1980).
27. Mao, C., LaBean, T. H., Reif, J. H. & Seeman, N. C. Logical computation using algorithmic self-assembly of DNA triple-crossover molecules. *Nature* **407,** 493–496 (2000).
28. Probst, J. C. Antisense oligodeoxynucleotide and ribozyme design. *Methods* **22,** 271–281 (2000).
29. Reardon, J. E. & Frey, P. A. Synthesis of undecagold cluster molecules as biochemical labeling reagents. 1. Monoacyl and mono[N-succinimidooxy)succinyl] undecagold clusters. *Biochemistry* **23,** 3849–3856 (1984).
30. Hermanson, G. T. *Bioconjugate Techniques* (Academic, San Diego, 1996).

Supplementary Information accompanies the paper on *Nature*'s website (http://www.nature.com).

Acknowledgements

We thank N. Afeyan, E. Lander and P. Matsudaira for discussions in the early stages of this work, and J.P. Shi for comments on the experimental work. This work was supported by DARPA and the MIT Media Lab TTT consortium.

Correspondence and requests for materials should be addressed to J.M.J. (e-mail: jacobson@media.mit.edu) or S.Z. (e-mail: shuguang@mit.edu).

15